Hydrodynamic Stability Analysis of CTEI

Jun-Ichi Yano

Hydrodynamic Stability Analysis of CTEI

jun-ichi Yano*

CNRM, UMR 3589 (CNRS), Météo-France, 31057 Toulouse Cedex, France

Corresponding author address: CNRM, Météo-France, 42 av Coriolis, 31057 Toulouse Cedex, France.

E-mail: jiy.gfder@gmail.com

ABSTRACT

A key question of the cloud-topped well-mixed boundary layer, consisting of stratocumulus clouds, is when and how this system transforms into trade-cumulus. For years, the cloud-top entrainment instability (CTEI) has been considered as a possible mechanism for this transition. However, being based on the local parcel analyses, the previous theoretical investigations are limited in applications. Here, a hydrodynamic stability analysis of CTEI is presented that derives the linear growth rate as a function of the horizontal wavenumber. For facilitating analytical progress, a drastically simplified treatment of the buoyancy perturbation is introduced, but in a manner consistent with the basic idea of CTEI. At the same time, the formulation is presented in a general manner that the effects of the wind shear can also be included. Under an absence of the wind shear, a well-mixed layer can become unstable due to the CTEI for horizontal scales larger than the order of the mixed–layer depth (*c.a.*, 1 km). The characteristic time scale for the growth is about one day, thus the CTEI is a relatively slow process compared to a typical deep-convective time scale of the order of hours. A major condition required for the instability is a higher efficiency of the evaporative cooling against a damping due to a mechanical mixing by cloud–top entrainment. Regardless of relative efficiencies of these two processes, the entrainment damping always dominates, and the CTEI is not realized in the small scale limit.

1. Introduction

The cloud-top entrainment instability (CTEI: Deardorff 1980) is considered a major potential mechanism for the transition of the stratocumulus to the trade cumulus over the marine subtropics (*cf.*, Stevens 2005 as an overview). The basic mechanism of CTEI resides on a possibility that an environmental air entrained into the cloud from the top can be dry enough so that its mixing with the cloudy-air leads to evaporation of the cloud water, and induces a sufficient negative buoyancy, leading to further entrainments of the environmental air from the cloud top. The process is expected to finally lead to a transition of stratocumulus into cumuli. A critical review of this process is provided by Mellado (2017), with the review itself even refuting CTEI as further discussed in the end in Sec. 5. Bretherton and Wyant (1997), and Lewellen and Lewellen (2002) propose decoupling as an alternative theoretical possibility.

However, the existing literature examines CTEI, mostly, in terms of a local condition, such as a buoyancy anomaly at the cloud top (inversion height). Such a parcel–based analysis leads to a criterion for instability in terms of a sign of buoyancy (*e.g.*, Deardorff 1980, Randall 1980, MacVean and Mason 1990, Duynkerke 1993). This type of approaches does not provide a full dynamical picture of the instability, including a quantitative estimate of a growth rate as a function of a horizontal scale (or a wavenumber), and a spatial structure of a preferred instability mode.

The qualitative nature of the existing criteria for CTEI makes it also difficult to test these criteria observationally (*cf.*, Albrecht *et al.* 1985, 1991, Kuo and Schubert 1988, Stevens *et al.* 2003, Mathieu and Lahellec 2005, Gerber *et al.* 2005, 2013, 2016). Most fundamentally, a finite time would be required for CTEI to realize. Unfortunately, bulk of existing theories does not tell how long we have to wait to observe CTEI.

A fundamental limitation of existing CTEI studies arises from a fact that these analyses concern only with a sign of a local buoyancy (or vertical eddy buoyancy flux), without properly putting it into a framework of the hydrodynamic instability ($cf.$, Drazin and Reid 1981). Such a dynamically consistent theoretical analysis of the instability couples a given local instability with a full hydrodynamics. It is a standard approach in the midlatitude large–scale dynamics to interpret the synoptic cyclones in this manner in terms of the baroclinic instabilities ($cf.$, Hoskins and James 2014). In the author's knowledge, a hydrodynamic stability analysis is still to be performed for CTEI, probably an exception of Mellado *et al.* (2009: $cf.$, Sec. 2.c). Thus is the goal of the study so that a growth rate of CTEI is obtained as a function of the horizontal scale.

A basic premise of the present study is to treat the evolution of the cloud–top inversion height with time explicitly so that, in principle, its evolution until an ultimate transform of stratocumulus into trade cumulus can be evaluated. A linear analysis performed herein is a first step towards this goal. As of any theoretical studies, the present analysis does not intend to provide a full answer to the problem. A more important purpose of the study is to show how dynamically–consistent instability analyses can be performed in problems of cloud–topped boundary layers, taking CTEI as an example. The author expects that more studies will follow along this line for better elucidating the dynamics of the cloud–topped boundary layers.

The present study considers an evolution of a resolved circulation under CTEI, which may be contrasted with some studies. The latter deal CTEI primarily as a process of generating kinetic energy for smaller–scale eddies, which directly contribute to vertical eddy transport at the top of the well–mixed layer associated with entrainment ($e.g.$, Lock and MacVean 1999, Katzwinkel *et al.* 2012). An overall approach of the present study may be compared with that for the mesoscale entrainment instability by Fiedler (1984: see also Fiedler 1985, Rand and Bretherton 1993). As a major difference, the entrainment induces negative buoyancy by evaporative cooling of clouds

in the present study, whereas Fielder considered an enhancement of cloudy–air positive buoyancy by entrainment of stable upper–level air. At a more technical level, the present study considers a change of the buoyancy jump crossing the inversion with time, but fixing the entrainment rate. In Fiedler (1984), in contrast, the main role of the inversion jump is to constraint the entrainment rate.

The model formulation, that couples a conventional parcel–based CTEI analysis with a full hydrodynamics, is introduced in the next section. A perturbation problem is developed in Sec. 3, and some simple solutions are presented in Sec. 4. The paper concludes with the discussions in the last section.

2. Formulation

A well-mixed boundary layer is considered. We assume that the mixed layer is cloud topped. However, the cloud physics, including the condensation, is treated only implicitly.

a. Rationales

An essence of CTEI is that a mixing of the free-troposphere air from the above with a cloudy air within stratocumulus leads to evaporation of cloud water due to a dry and relatively high temperature of the entrained free-atmospheric air, but the evaporative cooling, in turn, makes the entrained air colder than the surrounding stratocumulus-cloud air, leading to a convective instability that drives the evaporated mixed air further downwards (Deardorff 1980, Randall 1980). Though less frequently considered, a possible reverse process is an intrusion of the cloudy air from the stratocumulus cloud into the free troposphere (*e.g.*, MacVean and Mason 1990, Dyunkereke 1993). In this case, when the detrained air is moist enough, it can be more buoyant than the environment due to the virtual effect. Buoyancy induces a further ascent, the ascent leads to adiabatic cooling, the cooling may lead to further condensation of water vapor, and resulting condensative heating can drive the cloudy air further upwards.

The present study explicitly describes the deformation of the cloud–top inversion height with time, associated both with evaporation of cloudy air by cloud–top entrainment as well as intrusion of cloudy air into free troposphere. The resulting deformation may ultimately lead to transform of stratocumulus into trade cumulus. We will consider the associated processes under a drastically simplified mixed-layer formulation, but still taking into account of the basic CTEI processes just described. The drastic simplification facilitates the analysis of the coupling of these processes with a full dynamics in a form of hydrodynamic stability analysis.

Based on these rationales, a simple mixed–layer formulation for describing CTEI is introduced in the next subsection. It is coupled with a full hydrodynamics introduced in Secs. *c* and *d*.

b. A mixed-layer formulation for the buoyancy

We consider a well-mixed cloud-topped boundary layer with a depth (inversion height), z_i. The basic model configuration is shown in Fig. 1. As a key simplification, we assume that the buoyancy, b, is vertically well mixed. Clearly, this is a very drastic simplification. Under standard formulations (*e.g.*, Deardorff 1980, Schubert *et al.* 1979), the buoyancy anomaly is expressed by a linear relationship with the two conservative quantities, which are expected to be vertically well mixed. For these two quantities, we may take the equivalent potential temperature and the total water, for example. However, the buoyancy is not expected to be vertically well mixed, because the coefficients for this linear relationship are height dependent (*cf.*, Eq. 3.15 of Schubert *et al.* 1979, Eqs. 15 and 22 of Deardorff 1976). Thus, a drastic simplification in the present formulation is, more precisely, to neglect the height-dependence of these coefficients. However, we expect that drawbacks with these simplifications are limited, because only a perturbation of the buoyancy field is considered in the following. As a major consequence, a possibility of decoupling (Bretherton and Wyant 1997, Lewellen and Lewellen 2002) is excluded, thus the study focuses exclusively on CTEI.

Under these drastic simplifications, the buoyancy, b, in the well-mixed layer is described by

$$z_i(\frac{\partial}{\partial t}+<u>\frac{\partial}{\partial x})<b>=\overline{w'b'}_0-\overline{w'b'}_- - z_i Q_R \tag{2.1}$$

by following a standard formulation for the well-mixed boundary layer (*e.g.*, Eqs. 3.1 and 3.3 of Schubert *et al.* 1979, Eq. 2.1 of Stevens 2006). Here, the bracket, $<>$, designates a vertical average over the well-mixed layer. Strictly speaking, a deviation from a vertical average may exist, but we simply neglect these contributions in the formulation. A two–dimensional configuration has been assumed for a sake of simplicity. A full three–dimensional analysis would be substantially more involved without any practical benefits.

Here, we have introduced the variables as follows: t the time, x a single horizontal coordinate considered, u the horizontal wind velocity, $\overline{w'b'}$ the vertical buoyancy flux with the subscripts, 0 and $-$, designating the values at the surface and at the level just below the inversion (*i.e.*, z_{i-}), respectively; Q_R is the loss of buoyancy due to the radiative cooling over the well-mixed layer. Note that the buoyancy flux is discontinuous over the inversion associated with a discontinuity of the buoyancy (*cf.*, Fig. 1).

Under a standard formulation (*cf.*, Eqs. 1 and 2 of Deardorff 1980), the vertical eddy flux just below the inversion level may be expressed in terms of the entrainment rate, $w_e(>0)$, and a jump, $\Delta b = b_+ - <b>$, of the buoyancy over the inversion (with b_+ the free troposphere value at $z=z_{i+}$) as

$$\overline{w'b'}_- = -w_e \Delta b. \tag{2.2}$$

Here, standard CTEI criteria (Deardorff 1980, Randall 1980) require $\overline{w'b'}_- > 0$ or $\Delta b < 0$. When this condition is satisfied, the induced negative buoyancy is expected to induce further cloud–top entrainment, which induces further negative buoyancy: that is an essence of CTEI as described in the last subsection. Extensive CTEI literature focuses on defining this condition carefully due to a

subtle difference between the inversion buoyancy jump and an actual buoyancy anomaly generated by a cloud–top mixing ($cf.$, Duynkerke 1993). However, the present study bypasses this subtlety, being consistent with the already–introduced simplifications concerning the buoyancy.

In the following, we only consider the perturbations by setting:

$$z_i = \bar{z}_i + \eta,$$

$$< b > = < \bar{b} > + < b >',$$

where a bar and a prime designate equilibrium and perturbation values, respectively. An exception to this rule is the perturbation inversion height designated as η. For simplicity, we assume that w_e, $\overline{w'b'}_0$, and Q_R do not change by perturbations. See the next subsection for the discussions on the basic state, $\bar{z}_i$ and $< \bar{b} >$.

A perturbation on the buoyancy jump may be given by

$$\Delta b' = \left(\frac{d\bar{b}}{dz} \right) \eta - < b >' . \tag{2.3}$$

Here, the first term is obtained from a geometrical consideration (Fig. 2), assuming that the buoyancy profile above the inversion does not change by deepening of the mixed layer, thus $b'_+ = (d\bar{b}/dz)\eta$, where $d\bar{b}/dz\,(>0)$ is a vertical gradient of the free–troposphere buoyancy. Thus, a positive displacement, $\eta > 0$, of the inversion induces a positive buoyancy perturbation, $\Delta b' > 0$. We further extrapolate this formula downwards, thus $\Delta b' < 0$ with $\eta < 0$ ($i.e.$, entraining air into the mixed layer), as expected by evaporative cooling under the CTEI. Note that under the present formulation, entrainment directly induces a deformation of the inversion height, as a consequence of cloud evaporation. Both tendencies would induce further displacements of the inversion, and this positive feedback chain would induce an instability. To see this process more explicitly, the buoyancy equation must be coupled with a hydrodynamic system, as going to be introduced in next two subsections.

The second term in Eq. (2.3) simply states how a buoyancy perturbation, $< b >'$, of the mixed layer modifies the buoyancy jump, $\Delta b'$, at the inversion. As we see immediately below, these two terms have different consequences by entrainment.

Substitution of Eq. (2.3) into Eq. (2.2) reduces Eq. (2.1) into

$$[\bar{z}_i(\frac{\partial}{\partial t}+ < u > \frac{\partial}{\partial x}) + w_e] < b >' = \alpha\eta, \tag{2.4}$$

where

$$\alpha = w_e \left(\frac{d\bar{b}}{dz}\right) - Q_R \tag{2.5}$$

measures a feedback of the inversion height anomaly, η, on the buoyancy anomaly, $< b >'$. Here, we expect $\alpha > 0$. As already discussed above, the first term in Eq. (2.5) shows that displacements of the inversion tend to enhance the buoyancy perturbation. The second term is a negative radiative feedback, arising from the fact the total radiative cooling rate of the mixed layer changes by the inversion–height displacement. Negative feedback of radiation on CTEI has been pointed out by *e.g.*, Moeng and Schumann (1991), Moeng *et al.* (1995).

Eq. (2.4) contains the two competitive processes arising from the cloud–top entrainment: the first is a mechanical mixing as its direct consequence, that leads to a damping, as indicated by the last term in the left–hand side. The second is the evaporative cooling induced as an indirect consequence of the cloud–top entrainment, but more directly as a consequence of the inversion–height displacement, as seen in the right–hand side. The latter may induce instability. The first effect is independent of scales, whereas the second depends on scales, as further discussed with Eq. (3.8) below. The scale–dependence of the latter leads to a scale dependence of the CTEI growth rate as will be shown in Sec. 4.

c. Basic state

To introduce a hydrodynamics, we adopt a two-layer system with constant densities ($cf.$, Fig. 1), closely follozing a standard formulation for the analysis of the Kelvin–Helmholz instability as presented $e.g.$, in Ch. 4 of Drazin and Reid (1981). The first layer with a density, ρ_1, represents the well-mixed layer below, and the second with a density, ρ_2, the free troposphere above. To some extent, this formulation can be considered a local description of the dynamics around the top of the well-mixed layer (the inversion height), $z = z_i$, although the bottom (surface: $z = 0$) and the top ($z \to +\infty$) boundary conditions are considered explicitly in the following. A height dependence of the density can be introduced to this system, and so long as the density-gradient scale is much larger than a vertical scale of the interest, the given system is still considered a good approximation. Under this generalization, for the most parts in the following, the density values, ρ_1 and ρ_2, refer to those at the inversion height, $z = z_i$. We also assume that the horizontal winds, given by U_1 and U_2, are constant with height in each layer. Thus, we may re-set $U_1 =< u >$ in the formulation of the last subsection.

Here, an assumed sharp interface is a necessary simplification for treating the essential features of the CTEI in lucid manner, although both recent observational (Lenschow *et al.* 2000, Katzwinkel *et al.* 2012) and modeling (Moeng *et al.* 2005) studies show that the inversion actually constitutes a finite–depth layer with rich morphologies. Mellado *et al.* (2009) consider a Rayleigh-Taylor instability problem by inserting a positive density anomaly over this thin inversion layer. Their study may be considered an extension to three layers of the present formulation. However, in contrast to the present study, the fluid density is assumed a passive scalar and no possibility of its change associated with evaporation effects is considered.

We assume that the basic state is under a hydrostatic balance, thus the pressure field is given by

$$p = \begin{cases} p_i - \rho_1 g(z - z_i) & 0 \le z \le z_i \\ p_i - \rho_2 g(z - z_i) & z > z_i \end{cases} \tag{2.6}$$

where p_i is a constant pressure value at the inversion height.

The inversion height, z_i, is described by ($cf.$, Eq. 4 of Stevens 2002, Eq. 31 of Stevens 2006):

$$(\frac{\partial}{\partial t} + u_j \frac{\partial}{\partial x}) z_i = w + w_e \tag{2.7}$$

for both layers with $j = 1, 2$. Its steady basic state, $\bar{z}_i$, is defined by the balance:

$$\bar{w} + w_e = 0. \tag{2.8}$$

Here, $\bar{w}$ is a height-dependent background vertical velocity defined below. When $\bar{w} < 0$, we identify an equilibrium state at a certain height. Especially, when $\bar{w}$ is a monotonous function of the height, the equilibrium inversion height is unique. On the other hand, when $\bar{w} > 0$, there is no equilibrium height for the inversion, thus we may generalize above as

$$\dot{\bar{z}}_i = \bar{w} + w_e$$

with the rate, $\dot{\bar{z}}_i$, of change of the basic inversion height. In the latter case, the perturbation is applied against an unsteady state with $\dot{\bar{z}}_i \neq 0$. In the following, we further assume a constant background divergence, D, thus

$$\bar{w} = -Dz.$$

Finally, the basic state, $< \bar{b} >$, for the mixed-layer buoyancy is defined from Eq. (2.1) assuming a steady and homogeneous state. It transpires that the basic state is obtained from a balance between three terms in the right hand side. Unfortunately, deriving the basic-state explicitly for $< \bar{b} >$ is rather involved with a need of specifying the dependence of $\overline{w'b'}_0$ and Q_R on $< b >$ ($i.e.$,

specifications of physical processes). Here, we do not discuss this procedure, because this problem is, for the present purpose, circumvented by simply prescribing a mean state, $<\bar{b}>$. As it turns out, the value of $<\bar{b}>$ does not play any direct role in the instability problem.

d. Perturbation problem

For developing a perturbation problem, we assume that the perturbations satisfy the following boundary conditions (with the prime suggesting perturbation variables):

(i) $u' \to 0$ as $z \to +\infty$ (2.9a)

(ii) $w' = 0$ at the bottom surface, $z = 0$ (2.9b)

(iii) The pressure is continuous by crossing the inversion, $z = z_i$, thus

$$p'_1 - \rho_1 g\eta = p'_2 - \rho_2 g\eta \tag{2.9c}$$

at $z = \bar{z}_i$ after linearization. Furthermore, we may note that the perturbation equation for the inversion height is given by

$$(\frac{\partial \eta}{\partial t} + U_j \frac{\partial \eta}{\partial x}) = -D\eta + w' \tag{2.9d}$$

for $j = 1$ and 2.

The perturbation equations for the dynamics are given by

$$(\frac{\partial}{\partial t} + U_j \frac{\partial}{\partial x}) w'_j = -\frac{1}{\rho_j}\frac{\partial p'_j}{\partial z} + b'_j \tag{2.10a}$$

$$(\frac{\partial}{\partial t} + U_j \frac{\partial}{\partial x}) u'_j = -\frac{1}{\rho_j}\frac{\partial p'_j}{\partial x} \tag{2.10b}$$

for $j = 1$ and 2. Here, the buoyancy perturbation equation for the lower layer ($j = 1$) is given by setting $b'_1 = b'$ in Eq. (2.4). In the upper layer ($j = 2$), we simply set $b'_2 = 0$. Nonvanishing buoyancy perturbation in the upper layer (free troposphere) would contribute to the gravity-wave dynamics (*cf.*, Fiedler 1984). We simply neglect this contribution.

We further introduce the perturbation vorticity, ζ', and streamfunction, ψ', so that

$$\zeta' = \frac{\partial u'}{\partial z} - \frac{\partial w'}{\partial x} = \triangle \psi', \qquad w' = -\frac{\partial \psi'}{\partial x}, \qquad u' = \frac{\partial \psi'}{\partial z}, \tag{2.11a, b, c}$$

and for a later purpose, it is useful to note from Eqs. (2.11a, b):

$$\frac{\partial \zeta'}{\partial x} = -\triangle w'. \tag{2.11d}$$

The perturbation equations for the vorticity in both layers are obtained from Eqs. (2.10a, b):

$$(\frac{\partial}{\partial t} + U_1 \frac{\partial}{\partial x}) \zeta_1' = -\frac{\partial b_1'}{\partial x}, \tag{2.12a}$$

$$(\frac{\partial}{\partial t} + U_2 \frac{\partial}{\partial x}) \zeta_2' = 0. \tag{2.12b}$$

3. Stability Analysis

The perturbation problem is solved for the dynamics and the buoyancy separately in the following two subsections. Each leads to an eigenvalue problem.

a. Dynamics problem

The solutions for the upper layer is obtained in a relatively straightforward manner. From Eq. (2.12b), we find an only solution satisfying the condition of the vanishing perturbation flow towards $z \to +\infty$ (2.9a) is $\zeta_2' = 0$, thus

$$\triangle \psi_2' = 0,$$

whose solution consistent with the boundary condition (2.9a) is

$$\psi_2' = \hat{\zeta}_2 e^{ikx - k(z - \bar{z}_i) + \sigma t}.$$

Here, both the horizontal and the vertical scales are characterized by a single parameter, k, which is assumed to be positive; σ is a growth rate. It immediately follows that we may set

$$w_2' = \hat{w}_2 e^{ikx - k(z - \bar{z}_i) + \sigma t}, \tag{3.1a}$$

$$p_2' = \hat{p}_2 e^{ikx - k(z - \bar{z}_i) + \sigma t}, \tag{3.1b}$$

where $\hat{\zeta}_2$, $\hat{w}_2$, and $\hat{p}_2$ are the constants to be determined. The same conventions for the notation are also applied to the lower-layer solutions below.

The treatment of the lower layer is slightly more involved, because the vorticity is forced by the buoyancy. Nevertheless, by taking into account of the bottom boundary condition (2.9b), we may set:

$$\zeta_1' = \hat{\zeta}_1 \sin mz\, e^{ikx+\sigma t}, \tag{3.2a}$$

$$w_1' = \hat{w}_1 \sin mz\, e^{ikx+\sigma t}, \tag{3.2b}$$

$$p_1' = \hat{p}_1 \cos mz\, e^{ikx+\sigma t}, \tag{3.2c}$$

$$b_1' = \hat{b}_1 \sin mz\, e^{ikx+\sigma t}. \tag{3.2d}$$

Here, in the lower layer, the horizontal and the vertical scales are characterized by different wavenumbers, k and m. Note that at this stage, a possibility that the vertical wavenumber, m, is purely imaginary as in the upper layer is not excluded, but it is only excluded *a posteori*.

From Eq. (2.12a), we find

$$\hat{\zeta}_1 = -\frac{ik\hat{b}_1}{\sigma + ikU_1}.$$

It immediately follow from Eq. (2.11d) that

$$\hat{w}_1 = \frac{k^2}{(k^2+m^2)(\sigma+ikU_1)}\hat{b}_1 \tag{3.3a}$$

or

$$\hat{b}_1 = \frac{(k^2+m^2)(\sigma+ikU_1)}{k^2}\hat{w}_1. \tag{3.3b}$$

Note that Eq. (3.3a) corresponds to Eq. (2.53) of Fiedler (1984). Substitution of Eq. (3.3b) into Eq. (2.10a) further finds:

$$\hat{p}_1 = -\frac{\rho_1 m}{k^2}(\sigma+ikU_1)\hat{w}_1. \tag{3.4a}$$

A similar procedure applied to the upper layer leads to:

$$\hat{p}_2 = \frac{\rho_2}{k}(\sigma + ikU_2 + k\dot{\bar{z}}_i)\hat{w}_2. \tag{3.4b}$$

Application of the height perturbation equation (2.9d) to both layers leads to:

$$\hat{w}_1 = \frac{\sigma + ikU_1 + D}{\sin m\bar{z}_i}\hat{\eta}, \tag{3.5a}$$

$$\hat{w}_2 = (\sigma + ikU_2 + D)\hat{\eta}, \tag{3.5b}$$

and further substitution of Eqs. (3.5a) and (3.5b), respectively, into Eqs. (3.4a) and (3.4b) results in

$$\hat{p}_1 = -\frac{\rho_1 m}{k^2}(\sigma + ikU_1)(\sigma + ikU_1 + D)\frac{\hat{\eta}}{\sin m\bar{z}_i}, \tag{3.6a}$$

$$\hat{p}_2 = \frac{\rho_2}{k}(\sigma + ikU_2 + D)(\sigma + ikU_2 + k\dot{\bar{z}}_i)\hat{\eta}. \tag{3.6b}$$

Finally, substitution of Eqs. (3.6a, b) into the pressure boundary condition (2.9c) leads to an eigenvalue problem to be solved:

$$-\rho_1\frac{m}{k^2}(\sigma + ikU_1)(\sigma + ikU_1 + D)\cot m\bar{z}_i - \frac{\rho_2}{k}(\sigma + ikU_2 + D)(\sigma + ikU_2 + k\dot{\bar{z}}_i) - (\rho_1 - \rho_2)g = 0. \tag{3.7}$$

b. Buoyancy problem

Another eigenvalue problem is obtained from the buoyancy equation (2.4). By substitution of the general solutions, we obtain

$$[\bar{z}_i(\sigma + ikU_1) + w_e] < \sin mz > \hat{b}_1 = \alpha\hat{\eta}.$$

Here, the vertical average, $< \sin mz >$, is evaluated by

$$< \sin mz > = \frac{1}{\bar{z}_i}\int_0^{\bar{z}_i} \sin mz dz = -\frac{1}{m\bar{z}_i}\cos mz\Big|_0^{\bar{z}_i} = \frac{1 - \cos m\bar{z}_i}{m\bar{z}_i}.$$

Thus,

$$\hat{\eta} = \frac{1}{\alpha m\bar{z}_i}[\bar{z}_i(\sigma + ikU_1) + w_e](1 - \cos m\bar{z}_i)\hat{b}_1. \tag{3.8}$$

On the other hand, by combining Eqs. (3.3b) and (3.5a), we obtain

$$\hat{b}_1 = \frac{(k^2+m^2)(\sigma+ikU_1)(\sigma+ikU_1+D)}{k^2 \sin m\bar{z}_i}\hat{\eta}. \tag{3.9}$$

By substituting Eq. (3.9) into Eq. (3.8), we obtain the second eigenvalue problem

$$(k^2+m^2)(\sigma+ikU_1)(\sigma+ikU_1+D)[\bar{z}_i(\sigma+ikU_1)+w_e](1-\cos m\bar{z}_i) - \alpha m k^2 \bar{z}_i \sin m\bar{z}_i = 0. \tag{3.10}$$

As it turns out from the result of Sec. 4, a main balance in Eq. (3.9) that controls the system is:

$$(k^2+m^2)\hat{\eta} \sim \hat{b}_1, \tag{3.11}$$

thus the interface is displaced by the buoyancy more efficiently for larger horizontal scales (*i.e.*, the smaller k^2). A larger interface displacement, $\hat{\eta}$, leads to stronger evaporative cooling, thus the system becomes more unstable for the larger scales as will be found in Sec. 4.

c. Eigenvalue problems

As the analysis of the last two subsections show, the stability problem reduces to that of solving the two eigenvalue problems given by Eqs. (3.7) and (3.10). Here, the problem consists of defining two eigenvalues: the growth rate, σ, and the vertical wavenumber, m, of the mixed layer for a given horizontal wavenumber, k. Thus, two eigen-equations must be solved for these two eigenvalues.

In the following, we first nondimensionalize these two eigen-equations, then after general discussions, derive a general solution for the growth rate obtained from a nondimensionalized version of Eq. (3.7). This solution has a general validity. It also constitutes a self-contained solution when a coupling of the dynamical system considered in Secs. 2.*c* and 3.*a* with the buoyancy is turned off by setting $\alpha = 0$ in Eq. (2.4).

We note in Eq. (3.7) that a key free parameter of the problem is:

$$\mu = \frac{m}{k}\cot m\bar{z}_i. \tag{3.12a}$$

A key parameter in Eq. (3.10) is α, which is nondimensionalized into:

$$\tilde{\alpha} = (kg^3)^{-1/2}\alpha. \tag{3.12b}$$

Nondimensional versions of Eqs. (3.7) and (3.10) are given by

$$\mu(\tilde{\sigma}+i\tilde{U}_1)(\tilde{\sigma}+i\tilde{U}_1+\tilde{D})+\tilde{\rho}(\tilde{\sigma}+i\tilde{U}_2+\tilde{D})(\tilde{\sigma}+i\tilde{U}_2+\dot{\tilde{z}}_i)+(1-\tilde{\rho})=0, \tag{3.13a}$$

$$(1+\tilde{m}^2)(\tilde{\sigma}+i\tilde{U}_1)(\tilde{\sigma}+i\tilde{U}_1+\tilde{D})[\tilde{z}_i(\tilde{\sigma}+i\tilde{U}_1)+\tilde{w}_e](1-\cos\tilde{m}\tilde{z}_i)-\tilde{\alpha}\tilde{m}\tilde{z}_i\sin\tilde{m}\tilde{z}_i=0, \tag{3.13b}$$

where the nondimensional parameters and variables are introduced by:

$$\tilde{\sigma}=(kg)^{-1/2}\sigma, \quad \tilde{U}_j=(k/g)^{1/2}U_j, \quad \tilde{D}=(kg)^{-1/2}D, \tag{3.14a, b, c}$$

$$\tilde{\rho}=\rho_2/\rho_1, \quad \dot{\tilde{z}}_i=(k/g)^{1/2}\dot{z}_i, \quad \tilde{w}_e=(k/g)^{1/2}w_e, \tag{3.14d, e, f}$$

$$\tilde{m}=m/k, \quad \tilde{z}_i=k\bar{z}_i \tag{3.14h, g}$$

for $j=1, 2$. Note that a tilde $\tilde{}$ is added for designating the nondimensional variables.

A convenient general strategy for solving this set of eigen-equations would be to first solve Eq. (3.13a) for $\tilde{\sigma}$, and by substituting this result, solve Eq. (3.13b) for $\tilde{m}$. Note that Eq. (3.13a) is only the second order in respect to $\tilde{\sigma}$, thus an analytical solution for the latter is readily obtained. On the other hand, the resulting equation by substituting this result into Eq. (3.13b) is transcendental in respect to $\tilde{m}$. Thus the solution for $\tilde{m}$ must be sought numerically in general cases.

The general solution for the growth rate, $\tilde{\sigma}$, obtained from Eq. (3.13a) is:

$$\tilde{\sigma}=-i\tilde{U}_1\frac{\mu+\tilde{\rho}\Delta U}{\mu+\tilde{\rho}}-\frac{(\mu+\tilde{\rho})\Delta\tilde{D}+\tilde{\rho}\Delta\dot{\tilde{z}}_i}{2(\mu+\tilde{\rho})}\tilde{U}_1$$
$$\pm\frac{(\mu\tilde{\rho})^{1/2}\tilde{U}_1}{\mu+\tilde{\rho}}\{(1-\Delta U)^2(1-\tilde{R}i)+\frac{\tilde{\rho}}{4\mu}[\Delta\dot{\tilde{z}}_i+\frac{\mu+\tilde{\rho}}{\tilde{\rho}}\Delta\tilde{D}]^2+i(1-\Delta U)\Delta\dot{\tilde{z}}_i\}^{1/2}. \tag{3.15}$$

Here, for simplifying the final expression, some nondimensional parameters have been normalized by $\tilde{U}_1$:

$$\Delta U = \tilde{U}_2/\tilde{U}_1, \quad \Delta\dot{\tilde{z}}_i = \dot{\tilde{z}}_i/\tilde{U}_1, \quad \Delta\tilde{D} = \tilde{D}/\tilde{U}_1. \tag{3.16a, b, c}$$

Furthermore, a Richardson number, $\tilde{Ri}$, is introduced by:

$$\tilde{Ri} = \frac{(\mu+\tilde{\rho})(1-\tilde{\rho})}{\mu\tilde{\rho}\tilde{U}_1^2(1-\Delta U)^2} = \left(\frac{g}{k}\right)\frac{(\mu\rho_1+\rho_2)(\rho_1-\rho_2)}{\mu\rho_1\rho_2(U_1-U_2)^2}. \tag{3.16d}$$

Note especially that the system is unstable when $\tilde{Ri} < 1$ and the shear is strong enough. However, both the deepening, $\dot{\tilde{z}}_i(>0)$, of the mixed layer and the divergence, $\tilde{D}(>0)$ tend to suppresses the destabilization tendency.

4. Simple Solutions

a. Simplest case

The general solution (3.15) is clearly a rich source of instabilities, including a contribution of the shear with Ri, that is clearly worthwhile for further investigations (*cf.*, Brost *et al.* 1982, Kurowski *et al.* 2009, Mellado *et al.* 2009, Katzwinkel *et al.* 2012, Malinowski *et al.* 2013). However, for focusing on the CTEI problem, we turn off here the background winds $\tilde{U}_1 = \tilde{U}_2 = 0$. In this subsection, we consider the simplest case by further setting $\dot{\tilde{z}}_i = \tilde{D} = 0$. As a result, the growth rate obtained from Eq. (3.13a) reduces to:

$$\tilde{\sigma}^2 = -\frac{1-\tilde{\rho}}{\mu+\tilde{\rho}}. \tag{4.1a}$$

It suggests that when the system is unstable (*i.e.*, $\mathscr{R}(\tilde{\sigma}) > 0$), the mode is purely growing with no imaginary component. These simplifications also make the structure of the solution much simpler: we find immediately from Eq. (3.3a) that the mixed–layer vertical velocity, w_1', is in phase with the buoyancy perturbation, b_1', with the same sign, *i.e.*, $w_1' \sim b_1'$. Same wise, we find $w_1' \sim w_2' \sim \eta$ from Eqs. (3.5a, b), and $-p_1' \sim p_2' \sim \eta$ from Eqs. (3.6a, b).

Remainder of this subsection provides a self–contained mathematical description of how a closed analytic solution is derived. Readers who wish only to see the final results may proceed directly to the last two paragraphs of this subsection.

Eq. (3.13b) reduces to:

$$(1+\tilde{m}^2)\tilde{\sigma}^2(\tilde{z}_i\tilde{\sigma}+\tilde{w}_e)(1-\cos\tilde{m}\tilde{z}_i)-\tilde{\alpha}\tilde{m}\tilde{z}_i\sin\tilde{m}\tilde{z}_i=0. \tag{4.1b}$$

We immediately notice that by substituting an explicit expression (4.1a) for $\tilde{\sigma}^2$ into Eq. (4.1b), the latter further reduces to:

$$-(1+\tilde{m}^2)\frac{1-\tilde{\rho}}{\mu+\tilde{\rho}}(\tilde{z}_i\tilde{\sigma}+\tilde{w}_e)(1-\cos\tilde{m}\tilde{z}_i)-\tilde{\alpha}\tilde{m}\tilde{z}_i\sin\tilde{m}\tilde{z}_i=0. \tag{4.1c}$$

Here, a term with $\tilde{\sigma}$ is left unsubstituted for an ease of obtaining a final result later.

When the dynamics is not coupled with the buoyancy anomaly with $\tilde{\alpha}=0$, there are three possible manners for satisfying Eq. (4.1c): setting $\tilde{m}^2=-1$, $\tilde{\sigma}=-\tilde{w}_e/\tilde{z}_i$, or $\cos\tilde{m}\tilde{z}_i=1$. The first possibility leads to

$$\mu=\coth\tilde{z}_i.$$

In this case, μ is always positive so long as $\tilde{z}_i>0$. Thus, the system is always stable so long as it is stably stratified with $\tilde{\rho}<1$ according to Eq. (4.1a). The second gives a damping mode with the value of μ to be defined from Eq. (4.1a) by substituting this expression for $\tilde{\sigma}$. The last possibility leads to $\mu\to+\infty$, thus the system becomes neutrally stable.

On the other hand, when the dynamics is coupled with the buoyancy anomaly with $\tilde{\alpha}\neq 0$, the parameter μ may turn negative, thus the solution (4.1a) may become unstable. Here, recall the definition (3.12a) of this parameter, in which $\cot\tilde{m}\tilde{z}_i$ is a monotonously decreasing function of $\tilde{m}\tilde{z}_i$, and it changes from $+\infty$ to $-\infty$ as $\tilde{m}\tilde{z}_i$ changes from 0 to π, passing $\cot\tilde{m}\tilde{z}_i=0$ at $\tilde{m}\tilde{z}_i=\pi/2$. For focusing on the state with $\cot\tilde{m}\tilde{z}_i$ negative enough, we take the limit towards $\tilde{m}\tilde{z}_i\to\pi$, and set:

$$\tilde{m}\tilde{z}_i=\pi-\Delta\tilde{m}\tilde{z}_i. \tag{4.2}$$

We expect that $(0<)\Delta\tilde{m}\tilde{z}_i \ll 1$

Note that $\tilde{m}\tilde{z}_i = \pi$ corresponds to a solution that the perturbation vertical velocity vanishes exactly at the inversion level, $z = \bar{z}_i$, and as a result, the disturbance is strictly confined to the mixed layer without disturbing the inversion interface. In this case, no buoyancy anomaly is induced. Eq. (4.2) with $\tilde{m}\bar{z}_i < \pi$ suggests that the perturbation vertical velocity slightly intrudes into the free atmosphere.

Under the approximation (4.2), we obtain

$$\sin\tilde{m}\tilde{z}_i \simeq \Delta\tilde{m}\tilde{z}_i, \tag{4.3a}$$

$$\cos\tilde{m}\tilde{z}_i \simeq -1 \tag{4.3b}$$

as well as

$$\mu \simeq -\tilde{m}(\Delta\tilde{m}\tilde{z}_i)^{-1}, \tag{4.4}$$

where

$$\tilde{m} \simeq \pi/\tilde{z}_i = \pi/k\bar{z}_i \tag{4.5}$$

from the leading-order expression in Eq. (4.2). Note that from Eq. (4.4) and an assumption of $|\Delta\tilde{m}\tilde{z}_i| \ll 1$, we also expect $|\mu| \gg 1$. As a result, in the growth rate (4.1a), μ becomes dominant in denominator, and it reduces to:

$$\tilde{\sigma}^2 \simeq -\frac{1-\tilde{\rho}}{\mu} \simeq \frac{1-\tilde{\rho}}{\tilde{m}}\Delta\tilde{m}\tilde{z}_i. \tag{4.6}$$

By substituting all the approximations introduced so far into Eq. (4.1c):

$$2(1+\tilde{m}^2)\frac{1-\tilde{\rho}}{\tilde{m}}(\Delta\tilde{m}\tilde{z}_i)\,[\tilde{z}_i\tilde{\sigma} + \tilde{w}_e] - \tilde{\alpha}\tilde{m}\tilde{z}_i\Delta\tilde{m}\tilde{z}_i \simeq 0.$$

Two major terms share a common factor, $\Delta\tilde{m}\tilde{z}_i$, that can simply be dropped off, and a slight rearrangement gives:

$$\tilde{\sigma} + \frac{\tilde{w}_e}{\tilde{z}_i} \simeq \frac{\tilde{\alpha}}{2(1-\tilde{\rho})}\frac{\tilde{m}^2}{1+\tilde{m}^2}.$$

It leads to a final expression:

$$\tilde{\sigma} = -\tilde{D} + \tilde{A}, \tag{4.7}$$

where

$$\tilde{D} = \frac{\tilde{w}_e}{\tilde{z}_i} = k^{-1/2}\tilde{D}_0, \tag{4.8a}$$

$$\tilde{A} = \frac{\tilde{\alpha}}{2(1-\tilde{\rho})}\left(\frac{\tilde{m}^2}{1+\tilde{m}^2}\right) = k^{-1/2}\tilde{\varpi}(k)\tilde{A}_0 \tag{4.8b}$$

with the coefficients, $\tilde{D}_0$ and $\tilde{A}_0$, and a function, $\tilde{\varpi}(k)$, defined by:

$$\tilde{D}_0 = \frac{w_e}{g^{1/2}\bar{z}_i} \sim 10^{-4}\mathrm{km}^{-1/2}, \tag{4.9a}$$

$$\tilde{A}_0 = \frac{\alpha}{2(1-\tilde{\rho})g^{3/2}} \sim 10^{-4}\mathrm{km}^{-1/2}, \tag{4.9b}$$

$$\tilde{\varpi}(k) = [1 + (k\bar{z}_i/\pi)^2]^{-1}. \tag{4.9c}$$

Here, the order of magnitude estimates above are based on the values listed in the Appendix. By further substituting the expressions (4.8a, b) into Eq. (4.7):

$$\tilde{\sigma} \simeq (-\tilde{D}_0 + \tilde{\varpi}(k)\tilde{A}_0)k^{-1/2}, \tag{4.10}$$

Finally, the growth rate of the instability is given by

$$\sigma = g^{1/2}(-\tilde{D}_0 + \tilde{\varpi}(k)\tilde{A}_0) \tag{4.11}$$

after dimensionalizing the result (4.10) by following Eq. (3.14a). Here, $\tilde{\varpi}(k)$ is a decreasing function of k, and asymptotically $\tilde{\varpi}(k) \to 1$ and 0, respectively, towards $k \to 0$ and $+\infty$. Thus, the growth rate is asymptotically $\sigma \to g^{1/2}(-\tilde{D}_0 + \tilde{A}_0)$ and $\sigma \to -g^{1/2}\tilde{D}_0$, respectively, as $k \to 0$ and $+\infty$. It is seen that the sign of the growth rate with $k \to 0$ is defined by relative magnitudes of the mechanical entrainment, $\tilde{D}_0$, and the evaporative–cooling feedback, $\tilde{A}_0$. When the latter dominates the system is unstable in the large–scale limit, whereas when the former dominates it is damping. As the horizontal scale decreases (towards $k \to +\infty$), contribution of the

evaporative–cooling feedback gradually decreases, and the system becomes simply damping due to the mechanical entrainment effect. These points are visually demonstrated in Fig. **??** by plotting the growth rates for selected values of $\tilde{A}_0/\tilde{D}_0$. Here, the order of magnitude of the growth rate is estimated as $\sigma \sim g^{1/2}\tilde{D}_0 \sim g^{1/2}\tilde{A}_0 \sim 10^{-5}$ 1/s.

Recall that this solution is derived under an approximation of Eq. (4.2). Under this approximation, we seek a solution with convective plumes in the mixed layer slightly intruding into the free troposphere (*cf.*, Fig. **??**), as inferred by examining the assumed solution forms (3.2a–d). By combining this fact with the phase relations between the variables already identified (Eqs. 3.3a, b, 3.4a, b, 3.5a, b, 3.6a, b), we can easily add spatial distributions of the other variables to Fig. **??**, as already outlined after Eq. (4.1a) in Sec. 4.*a*.

b. Large-scale divergence effect

The simplest case considered in the last subsection illustrates well how a dynamically consistent CTEI arises as a natural extension of the Rayleigh-Taylor instability. However, the setting is rather unrealistic by neglecting a contribution of the large-scale divergence rate, $\tilde{D}$, to the problem. An existence of a positive finite divergence rate, $\tilde{D}$, defines the equilibrium height, $\bar{z}_i$, of the inversion under its balance with the entrainment is a crucial part of the well–mixed boundary–layer problem. Thus, in this subsection, we consider the modification of the problem by including a contribution of nonvanishing $\tilde{D}$.

The equation (3.13a) for the growth rate is modified to:

$$\tilde{\sigma}(\tilde{\sigma}+\tilde{D}) = -\frac{1-\tilde{\rho}}{\mu+\tilde{\rho}}, \tag{4.12a}$$

and its solution is

$$\tilde{\sigma} = -\frac{\tilde{D}}{2} \pm \left[\left(\frac{\tilde{D}}{2}\right)^2 - \frac{1-\tilde{\rho}}{\mu+\tilde{\rho}}\right]^{1/2}. \tag{4.12b}$$

Note that as suggested by the first term of the growth–rate expression (4.12b), a primarily role of the environmental descent is to damp the inversion–interface instability. However, as seen below, the full role of the environmental descent is subtler than just seen here.

The second eigenvalue equation (3.13b) reduces to:

$$(1+\tilde{m}^2)\tilde{\sigma}(\tilde{\sigma}+\tilde{D})(\tilde{z}_i\tilde{\sigma}+\tilde{w}_e)(1-\cos\tilde{m}\tilde{z}_i)-\tilde{\alpha}\tilde{m}\tilde{z}_i\sin\tilde{m}\tilde{z}_i=0. \tag{4.12c}$$

Note that the first two appearance of $\tilde{\sigma}$ in Eq. (4.12c) exactly constitutes the expression of the left hand side of Eq. (4.12a). A direct substitution of this expression leads to:

$$-(1+\tilde{m}^2)(\tilde{\sigma}+\frac{\tilde{w}_e}{\tilde{z}_i})\frac{1-\tilde{\rho}}{\mu+\tilde{\rho}}(1-\cos\tilde{m}\tilde{z}_i)-\tilde{\alpha}\tilde{m}\sin\tilde{m}\tilde{z}_i=0,$$

that is identical to Eq. (4.1c) obtained for the case without the background divergence, $\tilde{D}$. In other words, the effect of the environmental descent cancel out under the inversion–interface buoyancy condition. It immediately follows that we obtain the identical growth rate as the case without background divergence.

c. Under steady deepening by entrainment

Alternative consistent treatment is to turn off the environmental descent, *i.e.*, $\tilde{D}=0$, but instead, to assume that the well–mixed layer deepens steadily by entrainment, thus $\dot{\tilde{z}}_i\neq 0$ (and we will set $\dot{\tilde{z}}_i=\tilde{w}_e$ at the last stage). In this case, Eq. (3.13b) still reduces to Eq. (4.1b) as in Sec. 4.*a*. On the other hand, Eq. (3.13a) leads to:

$$\tilde{\sigma}^2=-\frac{1}{\mu+\tilde{\rho}}[\tilde{\rho}\dot{\tilde{z}}_i\tilde{\sigma}+(1-\tilde{\rho})]. \tag{4.13}$$

Substituting this expression for $\tilde{\sigma}^2$ into Eq. (4.1b), and only where $\tilde{\sigma}^2$ itself is found, leads to

$$-\frac{\tilde{\rho}\dot{\tilde{z}}_i}{\mu+\tilde{\rho}}(1+\tilde{m}^2)[\tilde{\sigma}^2+(\frac{1-\tilde{\rho}}{\tilde{\rho}\dot{\tilde{z}}_i}+\frac{\tilde{w}_e}{\tilde{z}_i})\tilde{\sigma}+\frac{1-\tilde{\rho}}{\tilde{\rho}\tilde{z}_i\dot{\tilde{z}}_i}\tilde{w}_e](1-\cos\tilde{m}\tilde{z}_i)-\tilde{\alpha}\tilde{m}\sin\tilde{m}\tilde{z}_i=0.$$

Finally, as before, we introduce approximations (4.3a, b) and (4.4) obtained under $\Delta\tilde{m}\tilde{z}_i\ll 1$. We retain only the terms with $O(\Delta\tilde{m}\tilde{z}_i)$. Thus, the term with $\tilde{\sigma}^2$ drops off in the above, because it is

expected to be $O(\Delta\tilde{m}\tilde{z}_i)$ by itself. After further reductions, we obtain

$$\tilde{\sigma} = (1 + \frac{\tilde{\rho}}{1-\tilde{\rho}} \frac{\tilde{w}_e \dot{\tilde{z}}_i}{\tilde{z}_i})^{-1} (\tilde{A} - \tilde{D}). \tag{4.14}$$

The result is the same as before apart from a prefactor containing $\dot{\tilde{z}}_i \neq 0$ to the front. The growth rate diminishes by this prefactor. The order of this correction is:

$$\frac{\tilde{\rho}}{1-\tilde{\rho}} \frac{\tilde{w}_e \dot{\tilde{z}}_i}{\tilde{z}_i} = \frac{\tilde{\rho}}{1-\tilde{\rho}} \frac{w_e^2}{g\bar{z}_i} \sim 10^{-6},$$

thus the contribution of the prefactor is negligible, and the same conclusion as before holds.

5. Discussions

A hydrodynamic stability analysis of the CTEI has been performed so that the growth rate of the CTEI is evaluated as a function of the horizontal wavenumber.

The degree of the CTEI is defined under a competition between the destabilization tendency due to the cloud–top evaporative cooling and the stabilization tendency due to the mechanical cloud–top entrainment. An important finding from the present study is to show that the entrainment effects can be separated into these two separate processes. Although the evaporative cooling associated with an intrusion of the free-troposphere air into the cloud is ultimately induced by the cloud top entrainment, the subsequent evolution of the inversion–interface can be described without directly invoking the entrainment, as presented in Sec. 2.*a*, by another parameter, α. The remaining role of the entrainment is a mechanical damping on the buoyancy perturbation as seen in the last term in the left–hand side of Eq. (2.14).

Obtained growth–rate tendencies with changing horizontal scales are consistent with qualitative arguments in Sec. 3 associated with Eq. (3.11). In the small scale limit, the damping effect due to the cloud–top entrainment dominates over the evaporative cooling, and as a result, the perturbation is always damping. In the large scale limit, instability may arise when the magnitude of the evaporative cooling rate is stronger than that of the entrainment as measured by a ratio between

the two parameters, $\tilde{A}_0$ and $\tilde{D}_0$, defined by Eqs. (4.9a, b). A transition from the small–scale damping regime to the large–scale unstable regime is defined by the scale $k\bar{z}_i/\pi \sim 1$, where the horizontal scale, π/k, of the disturbance is comparable to the mixed–layer depth, $\bar{z}_i$ ($\sim$ 1 km), with an exact transition scale depending on the ratio $\tilde{A}_0/\tilde{D}_0$. It can easily be shown that this ratio is essentially proportional to the vertical gradient of the buoyancy in the free troposphere, and a contribution of the entrainment rate is completely removed when a radiative feedback is set $Q_R = 0$ in Eq. (2.5). Thus, the CTEI considered under the present formulation does not strongly depend on the entrainment rate, when only these essential effects are retained to the problem.

The CTEI identified herein is inherently a large–scale instability, and a reasonably large domain is required to numerically realize it, as suggested by Fig. 3. This could be a reason why the evidence for the CTEI by LES studies so far is rather inconclusive (*e.g.*, Kuo and Schubert 1988, Siems *et al.* 1990, MacVean 1993, Yamaguchi and Randall, 2008). In these simulations, relatively small domain sizes (5 km square or less) are taken, that may prevent us from observing a full growth of the CTEI. The growth time scale for CTEI identified by the present analysis is also very slow, about an order of a day. With typically short simulation times with LESs (about few hours), that could be another reason for a difficulty for realizing a CTEI with these simulations. Direct numerical simulations (DNSs) by Mellado (2010), in spite of an advantage of resolving everything explicitly, are even in less favorable position for simulating a full CTEI due to an even smaller modeling domain. Unfortunately, dismissal of a possibility for CTEI by Mellado (2017) in his review is mostly based on this DNS result.

In contrast to these more recent studies, it may be worthwhile to note that an earlier study by Moeng and Arakawa (1980) identifies a reasonably clear evidence for CTEI over a high SST (sea surface temperature) region of their two–dimensional nonhydrostatic experiment with a 1000 km horizontal domain, assuming a linear SST distribution. A preferred scale identified by their ex-

periment is 30–50 km, qualitatively consistent with the present linear stability analysis, although it is also close to the minimum resolved scale in their experiment due a crude resolution. A time scale estimated from the present study is also consistent with a finding by Moeng and Arakawa (1980) that their CTEI–like structure develops taking over 24 hours. However, due to limitations of their simulations with parameterizations of eddy effects, a full LES is still required to verify their result. From an observational point of view, an assumption of horizontal homogeneity of the stratocumulus over such a great distance may simply be considered unrealistic in respect of extensive spatial inhomogeneity associated with the stratocumulus as realized in LESs (*e.g.*, Chung *et al.* 2012, Zhou and Bretherton 2019).

In this respect, it may be interesting to note that a recent observational study by Zhou *et al.* (2015) suggests a possibility of a certain cloud–top instability, if not CTEI, leading to a decoupling, which ultimately induces a transition to trade cumulus regime. We should realize that a rather slow time scale for CTEI identified by the present study may be another reason for difficulties of identifying it observationally. Previous observational diagnoses on CTEI criterions have been based on instantaneous comparisons (*e.g.*, Albrecht *et al.* 1985, 1991, Kuo and Schubert 1988, Stevens *et al.* 2003, Mathieu and Lahellec 2005, Gerber *et al.* 2005, 2013, 2016). A finite time lag could be a key missing element for a successful observational identification of CTEI. If that is the case, data analyses from a point of view of the dynamical system as advocated by Yano and Plant (2012) as well as Novak *et al.* (2017) becomes a vital alternative approach.

In the present study, a full solution is considered only for the simplest cases with no background wind. Nevertheless, a basic formulation is presented in fully general manner. Thus, a simple extension of the present study can consider rich possibilities of the mixed-layer inversion–interface instabilities under a coupling with the buoyancy anomaly. Especially, the present formulation allows us to explicitly examine a possibility of the Kelvin-Helmholtz instability over the mixed-layer

observationally suggested by Brost *et al.* (1982), Kurowski *et al.* (2009), Katzwinkel *et al.* (2012), Malinowski *et al.* (2013).

A question may still remain whether the present study actually considers the CTEI. In standard local analyses (*e.g.*, Lilly 1968, Deardorff 1980, Randall 1980), the main quantities considered are the signs of the mean vertical eddy buoyancy flux, $(\overline{w'b'})_-$, just below the inversion and the mean jump, Δb, of the buoyancy by crossing the inversion–interface. These parcel mixing analyses do not explicitly consider a finite displacement of the air masses. By focusing on the perturbation problem, these mean quantities do not play a role in the present analysis. Instead, the analysis is based on the formulation (2.3) for the perturbation on the buoyancy jump, $\Delta b'$. The present formulation estimates the buoyancy anomaly solely based on the inversion–interface displacement, η, which may only loosely be translated into a standard parcel–mass displacement framework. The mixing process remains totally implicit. Arguably, a full justification for the formulation (2.3) may be still to be developed. Nevertheless, an introduced simplified formulation is designed to well mimic the processes associated with the evaporative cooling associated with cloud–top entrainment albeit in a very crude manner.

A main problem with the present formulation could be, as pointed out in the Appendix, a rather small evaporative cooling rate estimated from the feedback parameter, α, defined by Eq. (2.5). However, the logic for the derivation of this definition based on the background buoyancy profile rather suggests that a strong buoyancy anomaly estimated by conventional parcel theories can exist only in a very transient manner. Mellado *et al.* (2009) examine this process by a linear stability analysis, and Mellado (2010) its full nonlinear evolution by DNSs. The present study, in turn, examines the subsequent possible development of a full instability after such an initial transient adjustment is completed.

A crucial aspect of the present formulation is to treat a deformation process of the inversion–interface explicitly, that could ultimately lead to transform of stratocumulus into trade cumulus as an expected consequence of CTEI. The main original contribution of the present study is, under a crude representation of CTEI, to present its linear growth rate as a function of the horizontal scale. More elaborated studies would certainly be anticipated, and the present study suggests that they are actually feasible. A main next challenge is to proceed to a fully nonlinear formulation, probably, by taking an analogy with the contour dynamics for the vortex dynamics ($cf.$, Dritschel 1989, Dritschel and Ambaum 1997), but by considering a full nonlinear evolution of the inversion height as a contour. Such as extension would be able to simulate a transformation of stratocumulus into trade cumulus in terms of a finite amplitude deformation of the inversion height. Both modeling and observational studies are further expected to follow.

acknowledgments

Chris Bretherton led my attention to Fiedler (1984), Bjorn Stevens to Mellado (2017), and Szymon Malinowski to Zhou *et al.* (2015).

Appendix: Typical physical values

Typical physical values (in the orders of magnitudes) of the problem are:

Acceleration of the gravity : $g \sim 10$ m/s^2

Entrainment rate : $w_e \sim 10^{-2}$ m/s ($cf.$, Stevens *et al.* 2003, Gerber *et al.* 2013)

Inversion height : $\bar{z}_i \sim 10^3$ m ($cf.$, Schubert *et al.* 1979)

Here, the values for w_e and $\bar{z}_i$ may be considered upper bounds, but they provide convenient rounded-up values. These two values further provide an estimate of a typical divergence rate:

$$D = w_e/\bar{z}_i \sim 10^{-5}\,1/\mathrm{s}$$

(*cf.*, Schubert *et al.* 1979).

The feedback rate, α, of the inversion height anomaly, η, to the buoyancy anomaly, $< b >'$, is estimated by substituting these typical values into Eq. (2.5) as:

$$\alpha \sim w_e \frac{d\bar{b}}{dz} \sim 10^{-2}\,\mathrm{m/s} \times 10^{-4}\,1/\mathrm{s}^2 \sim 10^{-6}\,\mathrm{m/s}^3,$$

where

$$\frac{d\bar{b}}{dz} \sim \frac{g}{\bar{\theta}} \frac{d\bar{\theta}}{dz} \sim 10\,\mathrm{m/s}^2 \times \frac{3 \times 10^{-3}\,\mathrm{K/m}}{300\,\mathrm{K}} \sim 10^{-4}\,1/\mathrm{s}^2,$$

and $\bar{\theta}$ is the basic state for the potential temperature. It further provides a rate of the change of buoyancy-anomaly by:

$$\alpha \frac{\eta}{z_i} \sim \alpha \sim 10^{-6}\,\mathrm{m/s}^3,$$

which leads to a buoyancy anomaly of the order $< b >' \sim 10^{-2}$ m/s^2 over a period of an hour ($\sim 10^4$ s). This value may be considered an underestimate compared with those obtained by local analyses: 0.01 m/s^2 $< b <$ 0.2 m/s^2 (Fig. 3 of Stevens 2002), -2 K $< b <$ 1 K (Fig. 2 of Duynkerke 1993). Implications are discussed in Sec. 5.

We also set $1 - \tilde{\rho} \simeq 10^{-2}$ assuming a jump of the temperature $\Delta T \simeq 3$ K crossing the inversion in estimating the parameter values in the main text.

References

Albrecht, B. A., R. S. Penc, and W. H. Schubert, 1985: An observational study of cloud-topped mixed layers. *J. Atmos. Sci.*, **42**, 800- 822

Albrecht, B. A., 1991: Fractional cloudiness and cloud-top entrainment instability. *J. Atmos. Sci.*, **48**, 1519–1525.

Bretherton, C. S., and M. C. Wyant, 1997: Moisture transport, lower-tropospheric stability, and decoupling of cloud-toppedboundary layers. *J. Atmos. Sci.*, **54**, 148–167.

Brost, R. A., J. C. Wyngaard, and D. H. Lenschow, 1982: Marine stratocumulus layers. Part II: Turbulence budget. *J. Atmos. Sci.*, **39**, 818–836.

Chung, D., G. Matheou, and J. Teixeira, 2012: Steady–state large–eddy simulations to study the stratocumulus to shallow cumulus cloud transition. *J. Atmos. Sci.*, **69**, 3265–3276.

Deardorff, J. W., 1976: On the entrainment rate of a stratocumulus-topped mixed layer. *Quator. J. Roy. Meteor. Soc.*, **102**, 563–582.

Deardorff, J. W., 1980: Cloud top entrainment instability. *J. Atmos. Sci.*, **37**, 131–147.

Drazin, P. G., and W. H. Reid, 1981: *Hydrodynamic Stability*, Cambridge University Press, Cambridge, 527pp

Dritschel, D. G., 1989: Contour dynamics and contour surgery: Numerical algorithms for extended, high-resolution modelling of vortex dynamics in two-dimensional, inviscid, incompressible flows. Comp. Phys. Rep., 10, 77–146.

Dritschel, D. G., and M. H. P.Ambaum, 1997: A contour-advective semi-Lagrangian numerical algorithm for simulating fine-scale conservative dynamical fields. *Q. J. Roy. Meteorol. Soc.*, **123**, 1097–1130.

Duynkerke, P. G., 1993: The stability of cloud top with regard to entrainment: Amendement of the theory of cloud-top entrainment instbility. *J. Atmos. Sci.*, **50**, 495–502.

Fiedler, B. H., 1984: The mesoscale stability of entrainment into cloud–topped mixed layers. *J. Atmos. Sci.*, **41**, 92–101.

Fiedler, B. H., 1985: Mesoscale cellular convection: Is it convection? *Tellus*, **37A**, 163–175.

Gerber, H., S. P. Malinwoski, J.-L. Brenguier, and F. Brunet, 2005: Holes and etrainment in stratocumulus. *J. Atmos. Sci.*, **62**, 443–459.

Gerber, H., G. Frick, S. P. Malinowski, H. Jonsson, D. Khelif, and S. K. Krueger, 2013: Entrainment rates and microphysics in POST stratocumulus. *J. Geophys. Res.*, **118**, 12094–12109.

Gerber, H., S. P. Malinowski, and H. Jonsson, 2016: Evaporative and radiative cooling in POST stratocumulus. *J. Atmos. Sci.*, **73**, 3877–3884.

Hoskins, B. J., I. N. James, 2014: *Fluid Dynamics of the Mid-Latitude Atmosphere*, Wiley, Blackwell, 432pp.

Katzwinkel, J., H. Siebert, and R. A. Shaw, 2012: Observation of a self–limiting, shear–induced turbulent inversion layer above marine stratocumulus. *Boundary-Layer Meteorol.*, **145**, 131–143.

Kurowski, M.J., S. Malinowski, and W. W. Grabowski, 2009: A numerical investigation of entrainment and transport within a stratocumulus-topped boundary layer. *Quator. J. Roy. Meteor. Soc.*, **135**, 77–92.

Kuo, H.-C., and W. H. Schubert, 1988: Stability of cloud-topped boundary layers. *Quator. J. Roy. Meteor. Soc.*, **114**, 887–916.

Lenschow, D. H., M. Zhou, X. Zeng, L. Chen, and X. Xu, 2000: Measurements of fine–scale structure at the top of marine stratocumulus. *Boundary-Layer Meteorol.*, **97**, 331–357.

Lewellen, D. C., and W. S. Lewellen, 2002: Entrainment and decoupling relations for cloudy boundary layers.*J. Atmos. Sci.*, **59**, 2966–2986.

Lilly, D. K., 1968: Models of cloud-topped mixed layers nunder a strong inversion. *Quator. J. Roy. Meteor. Soc.*, **94**, 292–309.

Lock, A. P., and M. K. MacVean, 1999: The generation of turbulence and entrainment by buoyancy reversal. *Quator. J. Roy. Meteor. Soc.*, **125**, 1017–1038.

MacVean, M. K., 1993: A numerical investigation of the criterion for cloud-top entrainment instability. *J. Atmos. Sci.*, **50**, 2481–2495.

MacVean, M. K., and P. J. Mason, 1990: Cloud-top entrainment instability through small-scale mixing and its parameterization in numerical models. *J. Atmos. Sci.*, **47**, 1012–1030.

Malinowski, S. P., H. Gerber, I. J.-L. Plante, M. K. Kopec, W. Kumala1, K. Nurowska, P. Y. Chuang, D. Khelif, and K. E. Haman, 2013: Physics of Stratocumulus Top (POST): turbulent mixing across capping inversion. *Atmos. Chem. Phys.*, **13**, 12171–12186.

Mathieu, A., and A. Lahellec, 2005: Comments on 'On entrainment rates in nocturnal marine stratocumulus' by Bjorn Stevens, Donald H. Lenschow, Ian Faloona, C.–H. Moeng, D. K. Lilly, B. Blomquist, G. Vali, A. Bandy, T. Campos, H. Gerber, S. Haimov, B. Morley, and D. Thornton (October B, 2003, **129**, 3469–3493). *Quator. J. Roy. Meteor. Soc.*, **131**, 1293–1295.

Mellado, J. P., 2010: The evaporatively driven cloud-top mixing layer. *J. Fluid Mech.*, **660**, 5–32.

Mellado, J. P., 2017: Cloud-top entrainment in stratocumulus clouds. *Ann. Rev. Fluid Mech.*, **49**, 145–169.

Mellado, J. P., B. Stevens, H.Schmidt, and N. Peters, 2009: Buoyancy reversal in cloud-top mixing layers. *Quator. J. Roy. Meteor. Soc.*, **135** 963–978.

Moeng, C.-H., and A. Arakawa, 1980: A numerical study of a marine subtropical stratus cloud layer and its stability. *J. Atmos. Sci.*, **37**, 2661–2676.

Moeng, C.-H., and U. Schumann, 1991: Composite structure of plumes in stratus-topped boundary layer. *J. Atmos. Sci.*, **48**, 2280–2291.

Moeng, C.-H., D. H. Lenschow, and D. A. Randall, 1995: Numerical investigations of the role of radiative and evaporative feedbacks in stratocumulus entrainment and breakup. *J. Atmos. Sci.*, **52**, 2869–2883.

Moeng, C.-H., B. Stevens, and P. P. Sullivan, 2005: Where is the interface of the stratocumulus-topped PBL? *J. Atmos. Sci.*, **62**, 2026–2631.

Novak, L., M. H. P. Ambaum, and R. Tailleux, 2017: Marginal stability and predator-prey behaviour within storm tracks. *Quator. J. Roy. Meteor. Soc.*, **143**, 1421-1433.

Rand, H. A., and C. S. Bretherton, 1993: Relevance of the mesoscale entrainment instability to the marine cloud–topped atmospheric boundary layer. *J. Atmos. Sci.*, **50**, 1152–1158.

Randall, D. A., 1980: Conditional instability of the first kind upside down. *J. Atmos. Sci.*, **37**, 125–130.

Schubert, W. H., and J. S. Wakefield, E. J. Steiner, and S. K. Cox, 1979: Marine stratocumulus convection. Part I: Governing equations and horizontally homogeneous solutions. *J. Atmos. Sci.*, **36**, 1286–1307.

Siems, S. T., C. S. Bretherton, M. B. Bakar, S. Shy, and R. E. Breidenthal, 1990: Buoyanyc reversal and cloud-top entrainment instability. *Quator. J. Roy. Meteor. Soc.*, **116**, 705–739.

Stevens, B., 2002: Entrainment in stratocumulus-topped mixed layers. *Quator. J. Roy. Meteor. Soc.*, **128**, 2663–2690.

Stevens, B., D. H. Lenschow, I. Faloona, C.–H. Moeng, D. K. Lilly, B. Blomquist, G. Vali, A. Bandy, T. Campos, H. Gerber, S. Haimov, B. Morley, and D. Thornton, 2003: On entrainment rates in nocturnal marine stratocumulus. *Quator. J. Roy. Meteor. Soc.*, **129**, 3469–3493.

Stevens, B., 2005: Atmospheric moist convection. *Ann. Rev. Earth Planet. Sci.*, **33**, 605–643.

Stevens, B., 2006: Bulk boundary-layer concepts for simplified models of tropical dynamics. *Theor. Comput. Fluid Dyn.*, **20**, 279–304.

727 Stevens, B., D. H. Lenschow, I. Faloona, C.-H. Moeng, D. K. Lilly, B. Blomquist, G. Vali, A.
728 Bandy, T. Campos, H. Gerber, S. Haimov, M. Morlkey, D. Thornton, 2003: On entrainmeznt rates
729 in nocturnal marine stratocumulus. *Quator. J. Roy. Meteor. Soc.*, **129**, 3469–3493.

730 Yamaguchi, T., and D. A. Randall, 2008: Large-eddy simulation of evaporatively driven entrain-
731 ment in cloud-topped mixed layers. *J. Atmos. Sci.*, **65**, 1481–1504.

732 Yano, J.-I., and R. S. Plant, 2012: Finite Departure from Convective Quasi-Equilibrium: Peri-
733 odic Cycle and Discharge-Recharge Mechanism. *Quator. J. Roy. Meteor. Soc*, **138**, 626–637.

734 Zhou, X., and C. S. Bretherton, 2019: Simulation of mesoscale cellular convection in ma-
735 rine stratocumulus: 2. Nondrizzling conditions. *Adv. Modeling Earth Sys.*, **11**, 3–18.
736 doi:10.1029/2019MS001448

737 Zhou, X., P. Kollias, and E. R. Lewis, 2015: Clouds, precipitation, and marine boundary layer
738 structure during the MAGIC field campaign. *J. Climate*, **28**, 2420–2442.

LIST OF FIGURES

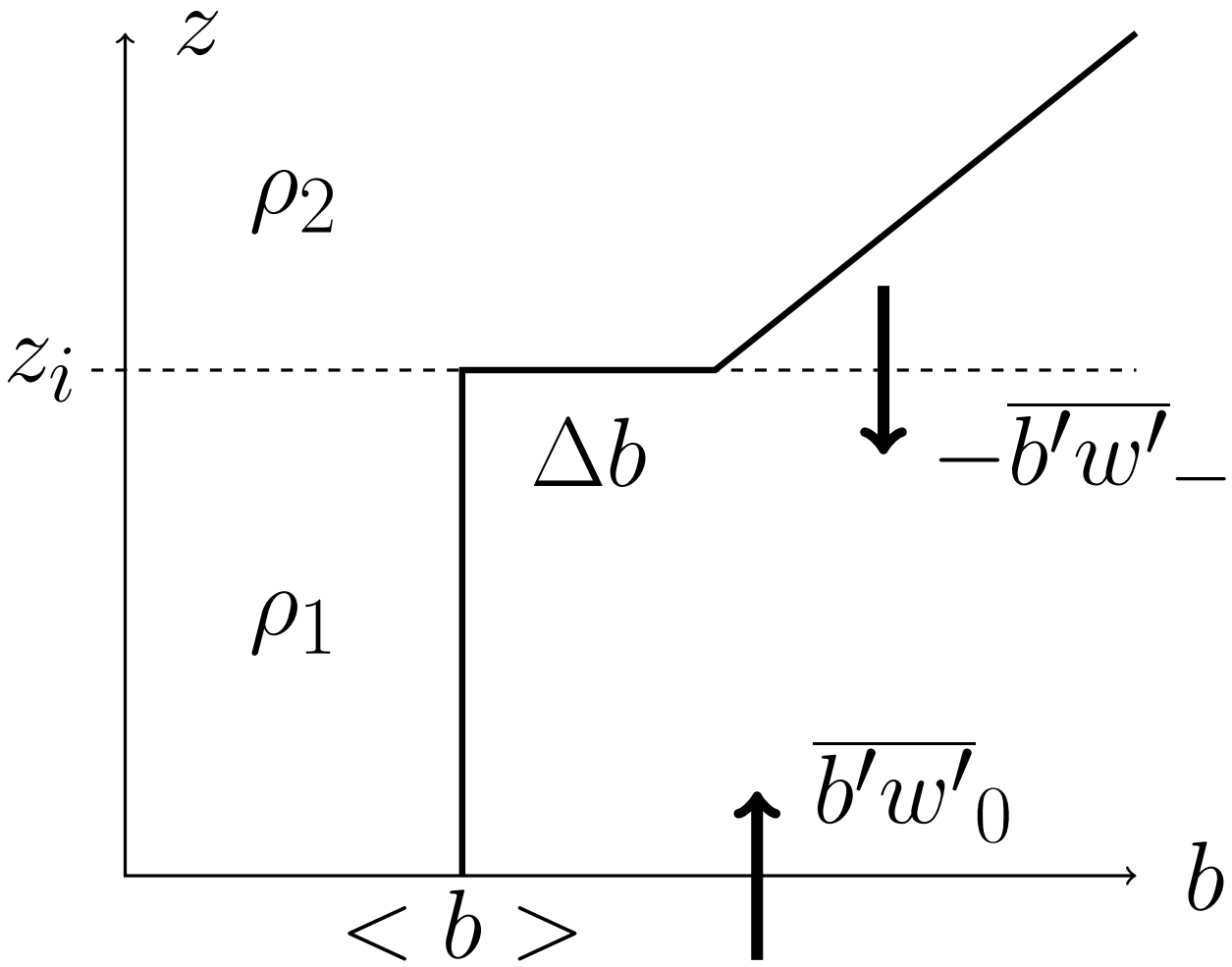

FIG. 1. Schematic configuration of the model.

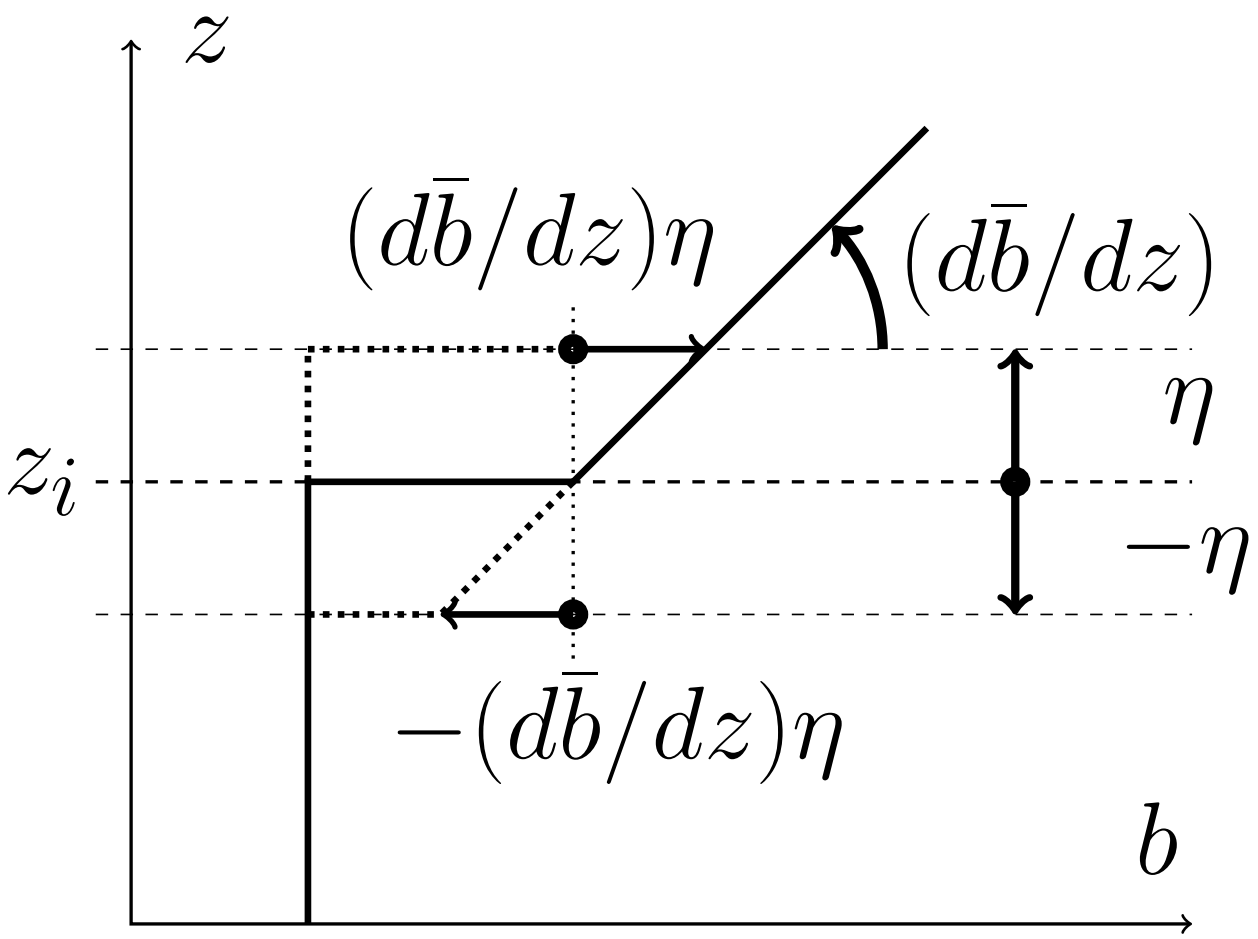

740 FIG. 2. Schematic presentation of a change, $\Delta b'$, of the buoyancy jump associated
741 with a change, η, of the inversion height.

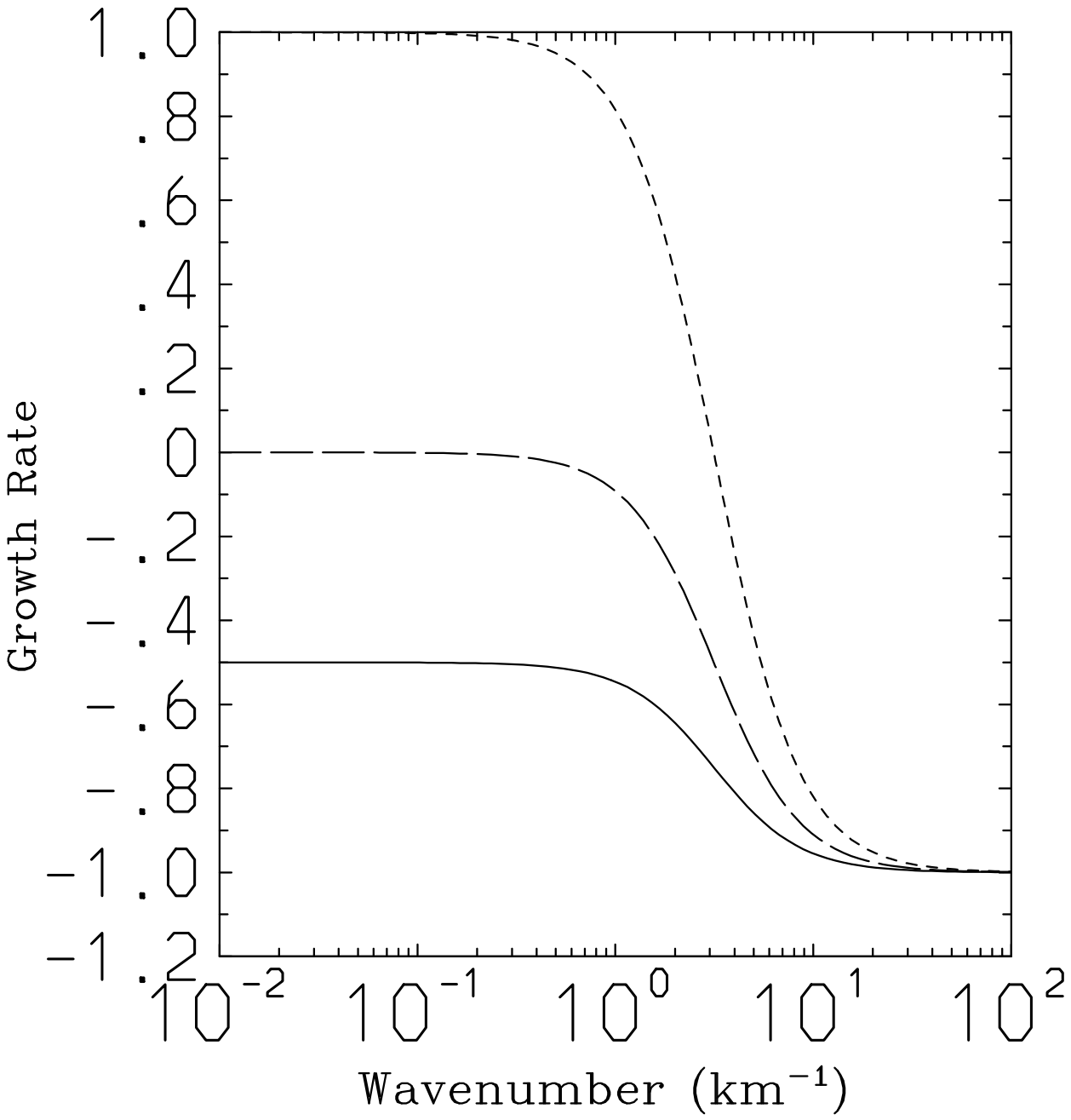

742 FIG. 3. Nondimensional growth rate, $\sigma/g^{1/2}\tilde{D}_0$ (Eq. 4.11), as a function of the
743 horizontal wavenumber, k (km^{-1}). The curves are with the fractional contribution
744 of the cloud-top re-evaporation of: $\tilde{A}_0/\tilde{D}_0 = 0.5$ (solid), $\tilde{A}_0/\tilde{D}_0 = 1$ (long-dash),
745 $\tilde{A}_0/\tilde{D}_0 = 2$ (short-dash). Note that the dimensional order of the growth rate is
746 $g^{1/2}\tilde{D}_0 \sim 1$ day^{-1}.

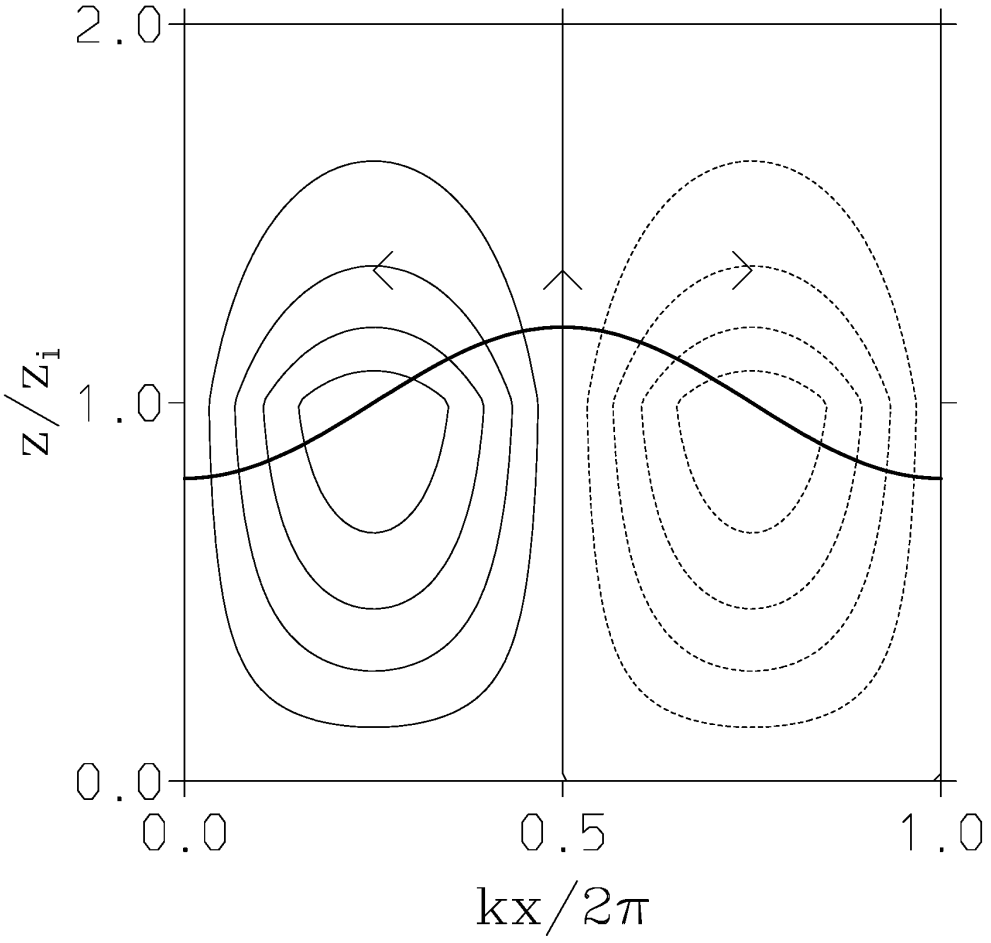

747 FIG. 4. Schematic structure of the perturbation solution: the streamfunction, ψ,
748 as contours, and the inversion--height deformation as a thick solid curve.